

β -decay properties of waiting point nuclei for astrophysical applications

Jameel-Un Nabi*, Munir Ahmad and Gul Daraz

March 21, 2017

Abstract

We report microscopic calculation of key β -decay properties for some of the crucial waiting point species having neutron closed magic shells 50 and 82. Our calculation bear astrophysical significance vis-à-vis speeding of the r -process. The β -decay properties include half-lives, energy rates of β -delayed neutrons and their emission probabilities, both under terrestrial and stellar conditions. We perform a pn-QRPA calculation with a separable multi-shell interaction and include both allowed and unique first-forbidden (U1F) transitions in our calculation. We compare our results with previous calculations and measured data. Our calculation is in good agreement with the experimental data. For certain cases, we noted a significant decrease in the half-life calculation with the contribution of U1F transitions. This is in contradiction to the shell model study where only for $N = 126$ waiting-point nuclei, the forbidden transitions were reported to significantly reduce the calculated half-lives. Our model fulfills the Ikeda sum rule for even-even cases. For odd- A cases the rule is violated by up to 15% for ^{125}Tc .

Keywords β -decay half-lives, pn-QRPA, Gamow-Teller transitions, U1F transitions, Ikeda sum rule, r -process.

PACS number(s) 23.40.2s, 26.30.1k, 97.60.Bw, 98.80.Ft

1 Introduction

Since the seminal paper on synthesis of elements in stars [1], our understanding of the nucleosynthesis process have greatly improved (for recent papers see e.g. [2, 3]). The r - and s -processes are the mastermind responsible for nucleosynthesis of heavy elements. The r -process mechanism basically requires the understanding of nuclear characteristics of hundreds of neutron-rich nuclide, mostly unknown. The weak interaction rates and reaction cross sections are amongst the key nuclear input data to affect the r -process calculation. The β -decay rates deserve a special mention as they are responsible for changing the nuclear specie during heavy element synthesis. At the same time r -process mechanism also demands accurate estimate

of other physical parameters including entropy, temperature, density and lepton-to-baryon ratio of the stellar matter. The physical conditions conducive for occurrence of r -process are relatively high temperatures (of the order of few GK) and high neutron densities ($> 10^{20} \text{ cm}^{-3}$) [1, 4, 5, 6, 7]. Under prevailing conditions the capturing process of neutrons takes place at a faster pace than the competing β -decay processes and many neutron-rich nuclei (with $S_n \lesssim 3 \text{ MeV}$) are produced. Nuclei possessing closed neutron shells of 50, 82 and 126 exhibit discontinuities in neutron separation energies because of stronger binding energy. Consequently the r -process matter flow decelerates and wait for occurrence of several β -decays to occur before the process of rapid neutron capture resumes. Peaks have been observed in the distribution abundances of r - mechanism at $N = 50, 82$ and 126 because of accumulation of matter at these waiting point nuclei. The calculated half-lives of β -decay for waiting point nuclei describes the time scale it takes the mass flow to transpose seed nuclei to larger nuclei in the third peak at around $A \sim 200$. Provided that the r - mechanism has enough duration time for β -flow equilibrium to built, the β -decay half-lives are proportional to the relative elemental abundances [8].

Unfortunately the experimental information for waiting point nuclei is scarce. For the neutron closed shells of $N = 50$ and 82 waiting point nuclei, the available half-lives are rather limited and insufficient [9, 10, 11, 12]. The scenario is expected to improve in near future with radioactive ion beam experiments at RIKEN [13] and GSI [14]. Hence for r -process simulations the required β -decay half-lives come primarily from theoretical estimations. An extensive tabulation of microscopic β -decay rates for a wide range of nuclei was reported by Klapdor-Kleingrothaus et al. [15]. Later, Staudt et al. [16, 17] and Hirsh et al. [18], used the proton-neutron quasiparticle random phase approximation (pn-QRPA) model, for the first time, to predict β -decay half-lives for a wide range of proton-rich and neutron-rich exotic nuclei. The r -process spectra of waiting point nuclei can be affected by the presence of low lying energy levels possessing different parities. This necessitates the incorporation of the first-forbidden (FF) chapter to the β -decay half-lives. The pn-QRPA model was used to estimate the FF contributions for a handful of nuclei for the first time by Homma et al. [19]. Later other models were used to estimate the FF contribution. These include, but are not limited to, the QRPA + gross theory [20], self-consistent density-functional + continuum QRPA [21] and more recently the large-scale shell model calculation [22]. Only a small percent of the total $3(N - Z)$ sum rule lie within the Q_β window for the neutron-rich nuclei participating in the r -process. The rest of the strength resides in the Gamow-Teller (GT) giant resonance located at much larger excitation energies. This may furnish explanation as to why different model calculations of β -decay half-lives may differ significantly without violating the sum rule.

Taking the weak-interaction rates to stellar domain is a next level calcu-

lation. Nabi and Klapdor-Kleingrothaus used the pn-QRPA approach and calculated stellar weak rates of $sd-$, $fp-$ and fpq -shell nuclei [23, 24, 25] for various astrophysical applications. The current pn-QRPA approach, using a separable interaction with a multi- $\hbar\omega$ space, makes possible a state-by-state calculation of weak interaction rates summing over Boltzmann-weighted, microscopically estimated GT strengths for all parent excited levels. This distinguishing feature of current calculation makes it unique amongst all calculations of stellar weak rates (including those using the independent particle model and shell model).

In the present work we report the GT strength distribution calculation, half-life calculation, stellar β -decay and positron emission rate calculations, energy rates of β -delayed neutron and corresponding neutron emission probabilities (P_n) for nuclei having neutron magic numbers ($N = 50$ and 82) using the pn-QRPA model. Ten waiting point nuclei (six having $N = 50$ and four having $N = 82$) were selected for this paper. In all cases we consider both the allowed GT and unique first-forbidden (U1F) transition contribution to the total weak rates. Non-unique transitions are also important. Currently we are working on codes to calculate non-unique contributions and their inclusion would be taken as a future assignment. We organize our paper in four sections. Section 2 describes the necessary pn-QRPA formalism. In Section 3, we show our results and present comparison with measurement and previous calculations. Conclusions and our key findings are drawn in Section 4.

2 Theoretical Formalism

The addition of all transition probabilities to levels in the daughter state j with energies E_j lying within the Q_β window gives the terrestrial half-life of β -decay.

$$T_{1/2} = \left(\sum_{0 \leq E_j \leq Q_\beta} 1/t_j \right)^{-1}, \quad (1)$$

where t_j shows the partial half-life for the allowed β -decay transition given by

$$f_0(Z, Q_\beta - E_j)t_j = \frac{D}{(g_A/g_v)^2 B(E_j)}, \quad (2)$$

here (g_A/g_v) is axial to vector coupling constant ratio, (numerical value is -1.254), D is a physical constant given by $D=2\pi^3\hbar^7 \ln 2/g_v^2 m_e^5 c^4$ (numerical value is 6295 s) and f_0 is the Fermi integral function (taking into account finite size effects and screening of nucleus, using the recipe of Gove and Martin [26]). The $B(E_j)$ gives the reduced transition probabilities (including GT and Fermi transitions). Our model includes GT force with separable particle-hole (ph) and particle-particle (pp) matrix elements. The two forces were characterized by strength parameter χ_{GT} and κ_{GT} , respectively. For

the pn-QRPA Hamiltonian, its model parameters, and calculation of reduced transition probabilities, we refer to [17, 18]. The formalism is not repeated here for space consideration.

For the U1F transitions the pp and ph matrix elements are given by

$$V_{pn,p'n'}^{ph} = +2\chi_{U1F} f_{pn}(\mu) f_{p'n'}(\mu), \quad (3)$$

$$V_{pn,p'n'}^{pp} = -2\kappa_{U1F} f_{pn}(\mu) f_{p'n'}(\mu), \quad (4)$$

where

$$f_{pn}(\mu) = \langle p | t_- r [\sigma Y_1]_{2\mu} | n \rangle, \quad (5)$$

is a single particle transition amplitude between Nilsson single particle states (deformed). Here μ values are labeled as, $\mu = 0, \pm 1$ and ± 2 (and represents the spherical component of the transition operator). Other symbols have regular meaning. The neutron and proton states possess different parities [19].

We varied the ph and pp strength interaction constant within the specified limits (ensuring the QRPA calculation does not "collapse"). Guidelines for choosing the interaction constants were taken from [19, 27]. The idea was to come up with an analytical formula for χ and κ that best reproduced the measured half-lives within 1σ deviation. Measured half-life data were taken from [28]. We obtained the following mass dependent relationship for these constants:

$$\chi_{GT} = 64.6/A \text{ MeV}; \chi_{U1F} = 64.6/A \text{ MeV fm}^{-2}, \\ \kappa_{GT} = 5.6/A \text{ MeV}; \kappa_{U1F} = 11.7/A \text{ MeV fm}^{-2}.$$

The deformation parameter was taken from the [29], while Q-values were taken from [28].

The stellar β -decay rates for allowed GT and U1F transitions from parent (i th level) to daughter (j th level) nucleus were determined using

$$\lambda_{ij}^\beta = \frac{m_e^5 c^4}{2\pi^3 \hbar^7} \sum_{\Delta J^\pi} g^2 f_{ij}(\Delta J^\pi) B_{ij}(\Delta J^\pi), \quad (6)$$

in the above equation $B_{ij}(\Delta J^\pi)$ and $f_{ij}(\Delta J^\pi)$ are the reduced transition probability and phase space factor respectively. For allowed transitions the reduced GT ($\Delta J^\pi = 1^+$) transition probabilities are given by

$$B(GT)_{ij} = \frac{1}{2J_i + 1} |\langle j || \sum_k t_-^k \vec{\sigma}^k || i \rangle|^2. \quad (7)$$

The reduced Fermi ($\Delta J^\pi = 0^+$) transition probabilities are given by

$$B(F)_{ij} = \frac{1}{2J_i + 1} |\langle j || \sum_k t_-^k || i \rangle|^2. \quad (8)$$

The phase space integral (f_{ij}) is an integral over total energy. For the case of β -decay it is given by (from here onwards we use natural units, $\hbar = m_e = c = 1$).

$$f_{ij} = \int_1^{w_m} w \sqrt{w^2 - 1} (w_m - w)^2 F(+Z, w) (1 - G_-) dw, \quad (9)$$

whereas for continuum positron capture phase space is given by

$$f_{ij} = \int_{w_l}^{\infty} w \sqrt{w^2 - 1} (w_m + w)^2 F(-Z, w) G_+ dw, \quad (10)$$

For the U1F transitions,

$$B_{ij}(\Delta J^\pi) = \frac{1}{12} z^2 (w_m^2 - 1) - \frac{1}{6} z^2 w_m w + \frac{1}{6} z^2 w^2, \quad (11)$$

where z is

$$z = 2g_A \frac{\langle j || \sum_k r_k [\mathbf{C}_1^k \times \boldsymbol{\sigma}]^2 \mathbf{t}_-^k || i \rangle}{\sqrt{2J_i + 1}}, \quad (12)$$

$$\mathbf{C}_{lm} = \sqrt{\frac{4\pi}{2l+1}} \mathbf{Y}_{lm}, \quad (13)$$

\mathbf{Y}_{lm} are the spherical harmonics. In case of U1F interaction, f_{ij} (phase space integral) were calculated using

$$f_{ij} = \int_1^{w_m} w \sqrt{w^2 - 1} (w_m - w)^2 [(w_m - w)^2 F_1(Z, w) + (w^2 - 1) F_2(Z, w)] (1 - G_-) dw, \quad (14)$$

where the upper limit of the integral gives the total β -decay energy given by $(w_m = m_p - m_d + E_i - E_j)$. w is the total energy of the electron including its rest mass. One should note that if the corresponding electron emission total energy, w_m , is greater than -1, then $w_l = 1$, and if it is less than or equal to 1, then $w_l = |w_m|$. The G_+ and G_- are the positron and electron distribution functions, respectively. The $F(\pm Z, w)$, $F_1(Z, w)$ and $F_2(Z, w)$ are the Fermi functions computed using the recipe of [26].

The high temperature inside the core of massive stars signifies that there is a finite probability of occupancy of parent excited levels in stellar scenario. Using the assumption of thermal equilibrium the occupation probability of i th state can be computed using

$$P_i = \frac{\exp(-E_i/kT)}{\sum_{i=1} \exp(-E_i/kT)}. \quad (15)$$

Finally stellar β -decay rate per unit time per nucleus was determined using

$$\lambda^\beta = \sum_{ij} P_i \lambda_{ij}^\beta. \quad (16)$$

A similar sum was performed to calculate continuum positron capture rates in stellar matter. Summations was carried out for all initial states as well as for final states until desired convergence were obtained in our rate calculation. In our calculation it was further assumed that all daughter excited states having energy larger than the neutron separation energy (S_n), decayed by neutron emission. The energy rate for neutron emission from daughter system was determined using

$$\lambda^n = \sum_{ij} P_i \lambda_{ij} (E_j - S_n), \quad (17)$$

for all $E_j > S_n$. The probability of β -delayed neutron emission, P_n , was calculated using

$$P_n = \frac{\sum_{ij'} P_i \lambda_{ij'}}{\sum_{ij} P_i \lambda_{ij}}, \quad (18)$$

where j' indicates the energy levels of the daughter nucleus with $E_{j'} > S_n$. The $\lambda_{ij(\prime)}$ in Eq. (17) and Eq. (18), represents the sum of positron capture and electron emission rates, for transition arising from $i \rightarrow j(j')$.

3 Results and discussion

In this section we are going to present the terrestrial β -decay half-lives, stellar weak rates, phase space and charge-changing strength distribution calculations, including both allowed GT and U1F transitions. The predictive power of the pn-QRPA model becomes more effective for smaller $T_{1/2}$ values (with increasing distance from the stability line) [18, 27] which justifies the usage of present model for β -decay calculations. We compare our calculation with several previous pioneering calculations [20, 21, 22, 30, 31] as well as against experimental data [28]. We multiplied results of pn-QRPA calculated strength by a quenching factor of $f_q^2 = (0.55)^2$ [32] in order to compare them with experimental data and prior calculations, and to later use them in astrophysical reaction rates.

The computed β -decay terrestrial half-lives for r -process waiting point nuclei having $N = 50$ and 82, including allowed GT and U1F contributions, are shown in Table 1. Here we also show the shell model calculations [33, 34] with only allowed GT contribution, the large scale shell model calculation [22] including both allowed GT and first-forbidden (FF) contributions and the QRPA calculation performed by [20] where the allowed GT part was calculated using the QRPA model and gross theory was employed to calculate the FF contribution. Experimental half-lives were taken from the

Table 1: Comparison of our computed β -decay half-lives for $N = 50$ and 82 r -process waiting point nuclei with previous calculations and experimental half-lives. Half-lives mentioned with an asterisk in the last column were adopted from [20].

Nucleus	A	SM [33, 34]	LSSM [22]	QRPA+ Gross Theory [20]		This work		Exp.[35]
		$T_{1/2}$ (GT)	$T_{1/2}$ (GT+FF)	$T_{1/2}$ (GT)	$T_{1/2}$ (GT+FF)	$T_{1/2}$ (GT)	$T_{1/2}$ (GT+U1F)	$T_{1/2}$
Fe	76	0.008	0.008	0.045	0.027	0.015	0.014	0.013*
Co	77	0.016	0.016	0.013	0.014	0.013	0.010	0.010*
Ni	78	0.127	0.150	0.477	0.224	0.210	0.152	0.140
Cu	79	0.222	0.270	0.430	0.157	0.273	0.239	0.220
Zn	80	0.432	0.530	3.068	1.260	0.910	0.634	0.550
Ga	81	0.577	1.030	1.568	1.227	1.509	1.457	1.217
Tc	125	0.009	0.010	0.009	0.009	0.031	0.008	0.008*
Ru	126	0.020	0.020	0.034	0.030	0.709	0.019	0.017*
Rh	127	0.028	0.028	0.022	0.020	0.109	0.074	0.070*
Pd	128	0.046	0.047	0.125	0.074	2.431	0.025	0.020

Table 2: Comparison of our computed β -decay half-lives for $N = 50$ r -process waiting point nuclei with previous calculations and experimental half-lives. $a \rightarrow [21]$ and $b \rightarrow [35]$.

Nuclei	A	Exp.	Borzov [21]	Möller [31]	Pfeiffer et al. [30]			This work	
		$T_{1/2}$	$T_{1/2}$ (GT+FF)	$T_{1/2}$ (GT)	$T_{1/2}$ (KHF)	$T_{1/2}$ (QRPA-1)	$T_{1/2}$ (QRPA-2)	$T_{1/2}$ (GT)	$T_{1/2}$ (GT+U1F)
Co	77	—	—	—	0.020	0.010	0.015	0.013	0.010
Ni	78	0.110 ^a	0.134	0.489	0.066	0.332	0.326	0.210	0.152
Cu	79	0.220 ^b	0.182	0.276	0.076	0.358	0.212	0.273	0.239
Zn	80	0.550 ^b	1.039	—	0.255	3.025	2.033	0.910	0.634
Ga	81	1.217 ^b	1.322	1.555	0.404	1.684	1.852	1.509	1.457

recent available atomic mass data evaluation of [35]. Table 2 shows a similar comparison of our calculated β -decay half-lives of $N = 50$ r -process waiting point nuclei with previous QRPA calculations and measured data. Here we compare with the self-consistent density-functional and continuum QRPA framework including the GT and FF transition calculation [21], a QRPA calculation using finite-range droplet model and folded-Yukawa single particle potential [31] and the QRPA calculations by [30]. For details of KHF, QRPA-1 and QRPA-2 calculations we refer to [30].

It may be seen from Table 1 and Table 2 that our calculated $T_{1/2}$ values are in very good comparison with the measured half-lives. Besides few $N = 50$ nuclei, the U1F contribution substantially lowers the calculated half-lives, specially for $N = 82$ cases.

The β -delayed neutron emission probabilities were also estimated by employing the QRPA [21, 30] and the shell model [22] approaches. Table 3 compares our pn-QRPA calculated β -delay neutron emission probabilities against previous calculations and experimental predictions. Noticeable differences between shell model and our calculated probabilities are seen in Table 3. Our numbers are in decent agreement with the QRPA calculations

of [30].

Table 3: Comparison between theoretical and experimental predictions of β -delayed neutron emission probability values for the selected waiting point nuclei.

Nucl.	A	Exp. [30]	LSSM [22]	Borzov [21]		Pfeiffer et al. [30]			This work
		P_n	P_n	P_n (GT)	P_n (GT+FF)	P_n (KHF)	P_n (QRPA-1)	P_n (QRPA-2)	P_n (GT+U1F)
Co	77	—	77.2	—	—	52.8	39.3	78.1	100.0
Ni	78	—	79	51.4	51.0	10.8	40.7	55.7	11.0
Cu	79	55	88.6	64.8	63.4	21.8	33.7	27.9	15.0
Zn	80	1	14.1	3.8	4.2	0.7	10.9	10.0	0.2
Ga	81	12.1	13	14.5	17.1	3.8	6.7	7.0	63.0

Table 4: Statistical data of pn-QRPA calculated GT strength distributions.

Waiting-point nuclei			Gamow-Teller Data			Ikeda Sum Rule	
Nucleus	Z	A	Centroid B(GT-)	Width B(GT-)	Σ B(GT-)	Calculated	Theoretical
Fe	26	76	48.0	5.1	72.1	72.0	72
Co	27	77	49.8	5.6	69.8	68.9	69
Ni	28	78	44.4	4.0	66.0	66.0	66
Cu	29	79	49.3	4.8	62.9	62.8	63
Zn	30	80	39.1	4.0	60.7	60.0	60
Ga	31	81	40.8	3.5	56.7	56.6	57
Tc	43	125	48.4	2.9	99.2	99.2	117
Ru	44	126	41.6	3.4	114.0	114.0	114
Rh	45	127	45.9	3.2	97.9	97.9	111
Pd	46	128	38.8	2.9	108.4	108.0	108

The total GT strength (in β -decay direction), centroid and width of calculated GT strength distributions for the $N = 50$ and 82 waiting point nuclei using our pn-QRPA model are shown in Table 4. The table reveals placement of GT centroid at high excitation energies in daughter nuclei. This necessitates the calculation of charge-changing transitions up to high excitation energies in daughter. Only a large model space (up to 7 major shells) made this calculation in the present formalism possible. Shown also in Table 4 is the comparison of our calculated Ikeda sum rule with the theoretical prediction (which is model independent). It may be seen that the Ikeda sum rule is fulfilled for even-even cases. For odd-A cases the compliance is 85% and 88% for ^{125}Tc and ^{127}Rh , respectively. For remaining odd-A cases the compliance is greater than 99%.

Moving on from terrestrial to stellar environment, we investigate the electron emission (β^-) rates and (continuum) positron capture (e^+) rates for density range ($10 - 10^{11} \text{ g.cm}^{-3}$) and temperature range ($0.01 \leq T_9 \leq 30$, where T_9 gives core temperature in units of GK), for our selected ten r -process waiting point nuclei. Figs. 1- 10 show the calculated weak rates for the ten selected nuclei. Each figure consists of three panels. The upper panel shows the calculated sum of positron capture and electron emission rates in

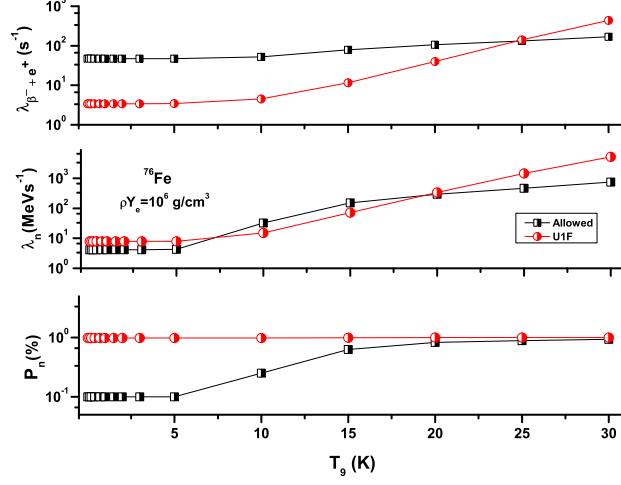


Figure 1: The pn-QRPA calculated β^- decay and positron capture rates (upper panel), energy rates of β -delayed neutron (middle panel) and their emission probabilities (bottom panel) for ^{76}Fe as a function of core temperature at stellar density of 10^6 g.cm^{-3} . The allowed GT and U1F contributions are shown separately.

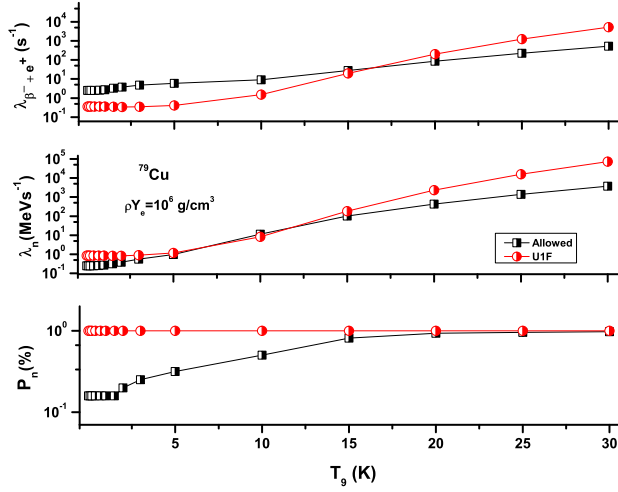


Figure 2: Same as Fig. 1 but for ^{79}Cu .

stellar environment as a function of core temperature. It is to be noted that all parent excited states are contributing to the calculated (β^- and e^+) rate calculation (see Eq. (16)). The middle panel depicts the calculated energy rates of β -delayed neutron in units of MeV.s^{-1} . The bottom panel shows the calculated β -delayed neutron emission probabilities. Within the

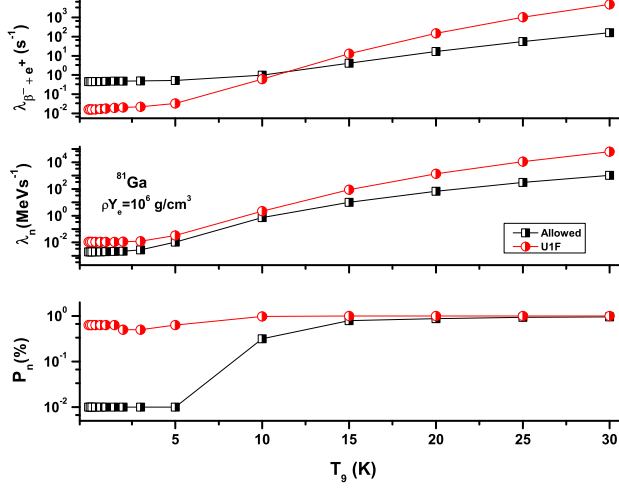


Figure 3: Same as Fig. 1 but for ^{81}Ga .

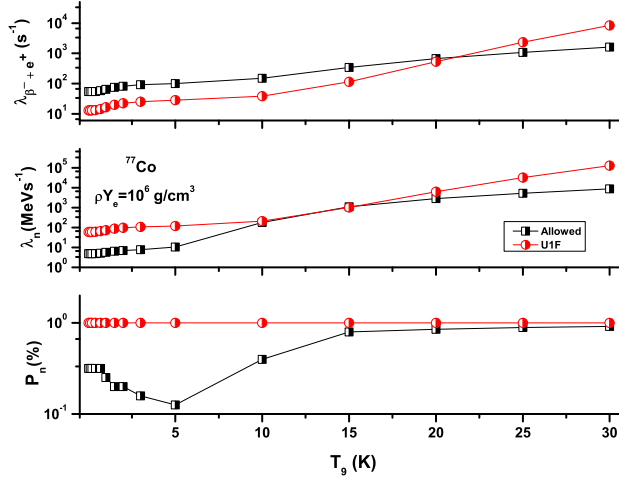


Figure 4: Same as Fig. 1 but for ^{77}Co .

Q_β window, the β -delayed neutron emission probabilities (P_n) are required for the description of β strength functions and neutron separation energies. In all panels we show the allowed GT and U1F contributions separately. All weak rates were calculated at a fixed stellar density of 10^6 g.cm^{-3} (simulating an intermediate value of core density under stellar conditions).

For the intermediate density, the allowed rates in upper panel of Figs. 1-3, are up to an order of magnitude bigger than the U1F rates at low stellar

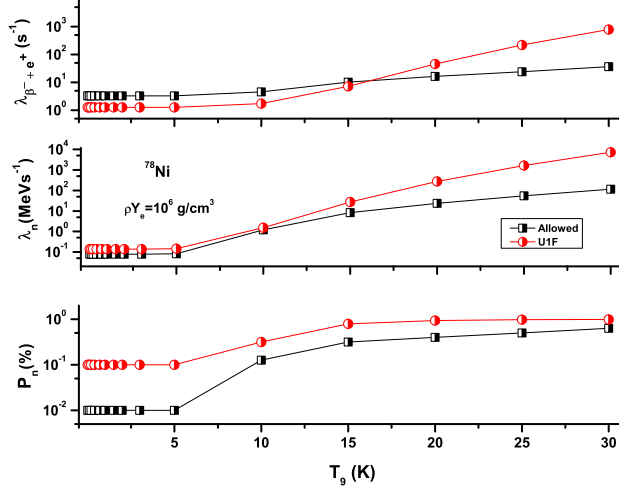


Figure 5: Same as Fig. 1 but for ^{78}Ni .

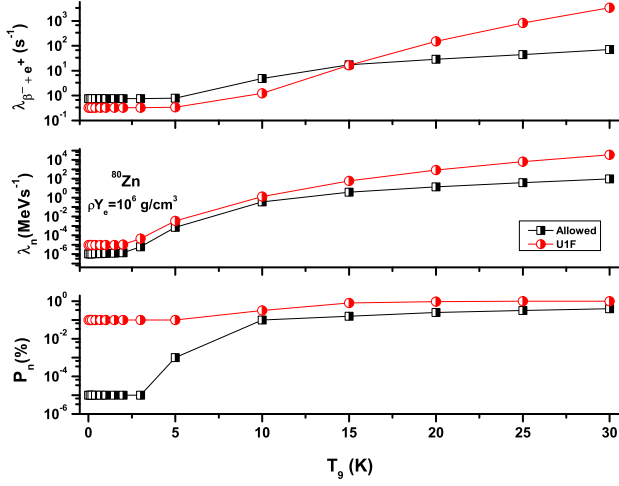


Figure 6: Same as Fig. 1 but for ^{80}Zn .

temperatures for ^{76}Fe , ^{79}Cu and ^{81}Ga , respectively. It is further noted that with the increase of core temperature the U1F rates increase at a faster pace and surpass the allowed rates at high T_9 values. At low core temperatures, more β -delayed neutrons are released due to U1F transitions than due to GT transitions. Accordingly, at low temperatures the energy rates of β -delayed neutron, due to U1F transitions, is factor 2, factor 3 and up to an order of magnitude bigger for ^{76}Fe , ^{79}Cu and ^{81}Ga , respectively. The energy rates

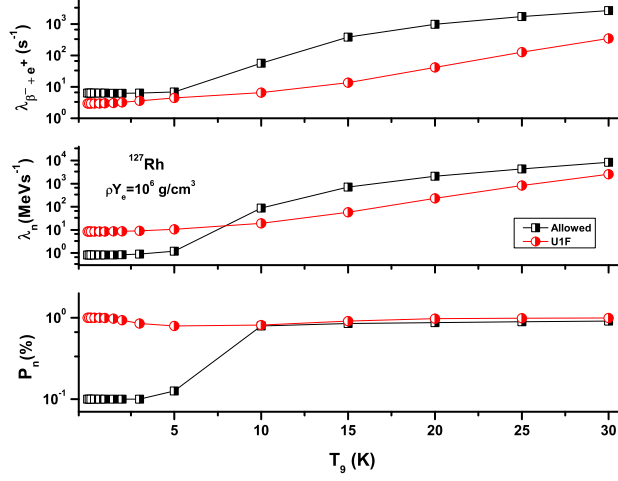


Figure 7: Same as Fig. 1 but for ^{127}Rh .

due to U1F transitions are more than an order of magnitude bigger at high stellar temperatures. The corresponding emission probabilities due to U1F transitions are also appreciably greater as can be seen in bottom panel of Figs. 1- 3. At $T_9 = 30$ it is almost certain that β -delayed neutrons would be emitted, both due to allowed GT and U1F transitions.

Figs. 4- 6 show similar results for the waiting point nuclei ^{77}Co , ^{78}Ni and ^{80}Zn , respectively. Here the allowed β -decay rates are factor 3 – 4 bigger than the corresponding U1F rates at low temperatures. At high stellar temperatures the U1F rates supersede the GT rates by more than an order of magnitude. The energy rates due to U1F transitions are an order of magnitude bigger at low temperatures and even bigger at high T_9 values.

Moving on to $N = 82$ waiting point nuclei, Fig. 7 shows the pn-QRPA calculated weak rates for ^{127}Rh . Here the allowed β -decay rates are factor 2 bigger than U1F rates at low temperatures and more than order of magnitude bigger at high temperatures. There is no crossing over between GT and U1F β -decay rates as witnessed in previous figures (Figs. 1- 6). However this crossing over of rates is seen in the case of energy rates where U1F rates is an order of magnitude bigger at low temperatures and factor 3 – 5 smaller at high stellar temperatures.

The weak rate calculations for remaining three $N = 82$ r -process waiting point nuclei, ^{125}Tc , ^{126}Ru and ^{128}Pd are presented in Figs. 8- 10, respectively. The β -decay rates due to U1F transitions are factor 3 bigger than due to allowed transitions for ^{125}Tc at low stellar temperatures (Fig. 8). At high temperatures the allowed and U1F β -decay rates compete well. The middle panel shows that the energy rates due to U1F rates are an order of magnitude

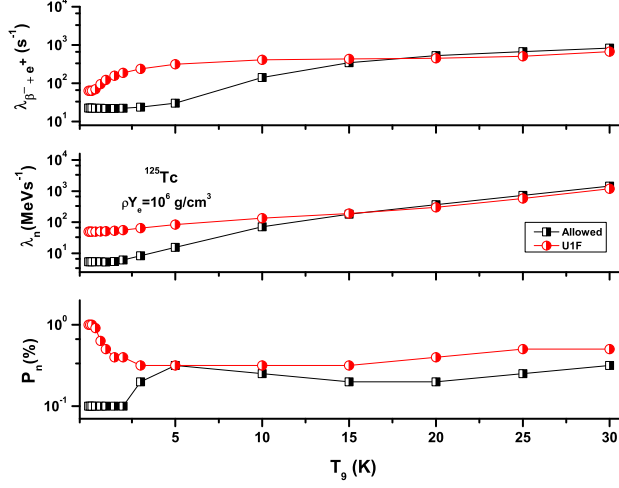


Figure 8: Same as Fig. 1 but for ^{125}Tc .

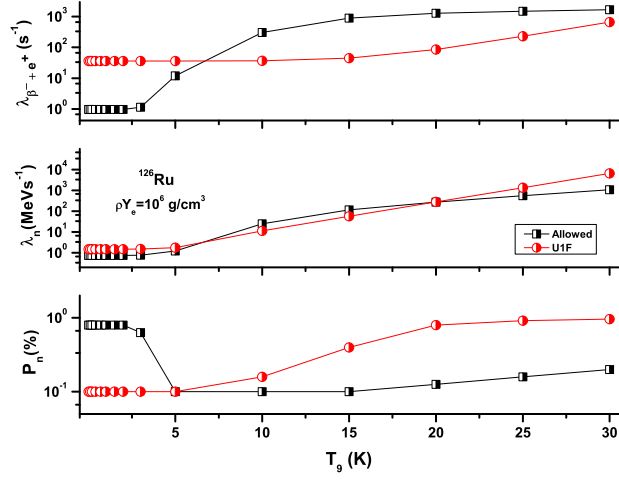


Figure 9: Same as Fig. 1 but for ^{126}Ru .

bigger at low temperatures and approach the allowed GT energy rates at high temperatures. Upper panels of Fig. 9 and Fig. 10 show that the U1F β -decay rates are an order of magnitude bigger at low temperatures. The middle panels show that UIF energy rates are factor 2 – 6 bigger than allowed energy rates at low and high T_9 values.

At low stellar temperatures, positron capture rates may safely be neglected in comparison to β -decay rates. Only at high core temperatures

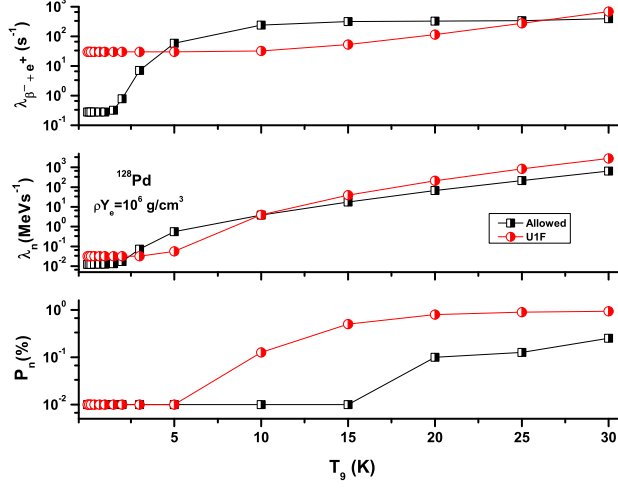


Figure 10: Same as Fig. 1 but for ^{128}Pd .

($kT > 1$ MeV), positron appears via e^-e^+ pair creation. Positron capture rates becomes at par with β -decay rates at $T_9 = 30$ (in fact for ^{81}Ga they are an order of magnitude bigger than β -decay rates). In general the weak rates are product of phase space and reduced transition probabilities (directly linked with strength distribution functions). The reason for the behavior of pn-QRPA calculated weak rates depicted in Figs. 1- 10 may be traced to the allowed and U1F strength distributions and phase space calculations which we discuss next.

In Fig. 11 and Fig. 12, we show the phase space calculation for allowed and U1F transitions as a function of core temperature for $N = 50$ and $N = 82$ waiting point nuclei, respectively, at stellar density of 10^6 g.cm^{-3} . We chose the same density at which we showed the calculation of weak rates earlier.

The phase space calculation for $N = 50$ nuclei in Fig. 11 displays certain distinctive features. At low stellar temperatures, the U1F phase space is bigger by as much as an order of magnitude compared to the allowed phase space. ^{81}Ga is an exception where the allowed phase space is bigger roughly by an order of magnitude at $T_9 = 0.01$. The phase space initially increases at a fast pace till the core temperature approaches $T_9 = 1$. Beyond this temperature the phase space remains almost constant till $T_9 = 30$. At high temperatures the two phase spaces are roughly the same for ^{76}Fe , ^{77}Co , ^{78}Ni and ^{79}Cu . Allowed phase space is bigger (smaller) than U1F phase space at high temperatures for ^{80}Zn (^{81}Ga).

Fig. 12 shows few similarity of phase space calculation for $N = 82$ waiting point nuclei with the $N = 50$ case. Once again the allowed phase space is

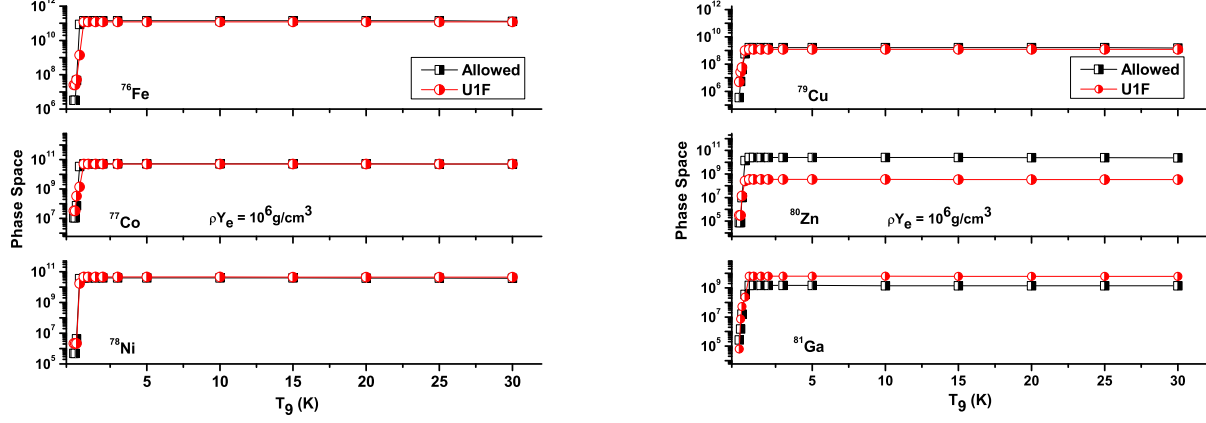


Figure 11: Calculated phase space for allowed (GT) and unique first-forbidden (U1F) β -decay for $N = 50$ waiting point nuclei as a function of stellar temperature at stellar density of 10^6 g.cm^{-3} .

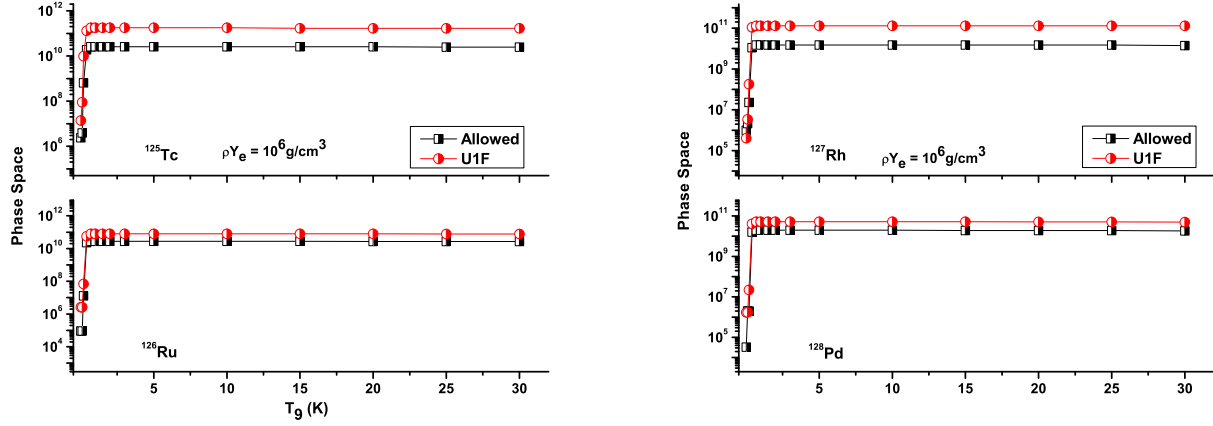


Figure 12: Same as Fig. 11 but for $N = 82$ waiting point nuclei.

orders of magnitude smaller than the U1F phase space at low temperatures (with the exception of ^{127}Rh). The rate of increase of phase space with temperature is rapid till $T_9 = 1$ and almost none beyond this temperature. In all four cases we note that the U1F phase space is bigger by as much as one order of magnitude at all temperatures (the only exception being ^{127}Rh at $T_9 = 0.01$). This is one reason why U1F transitions contribute significantly

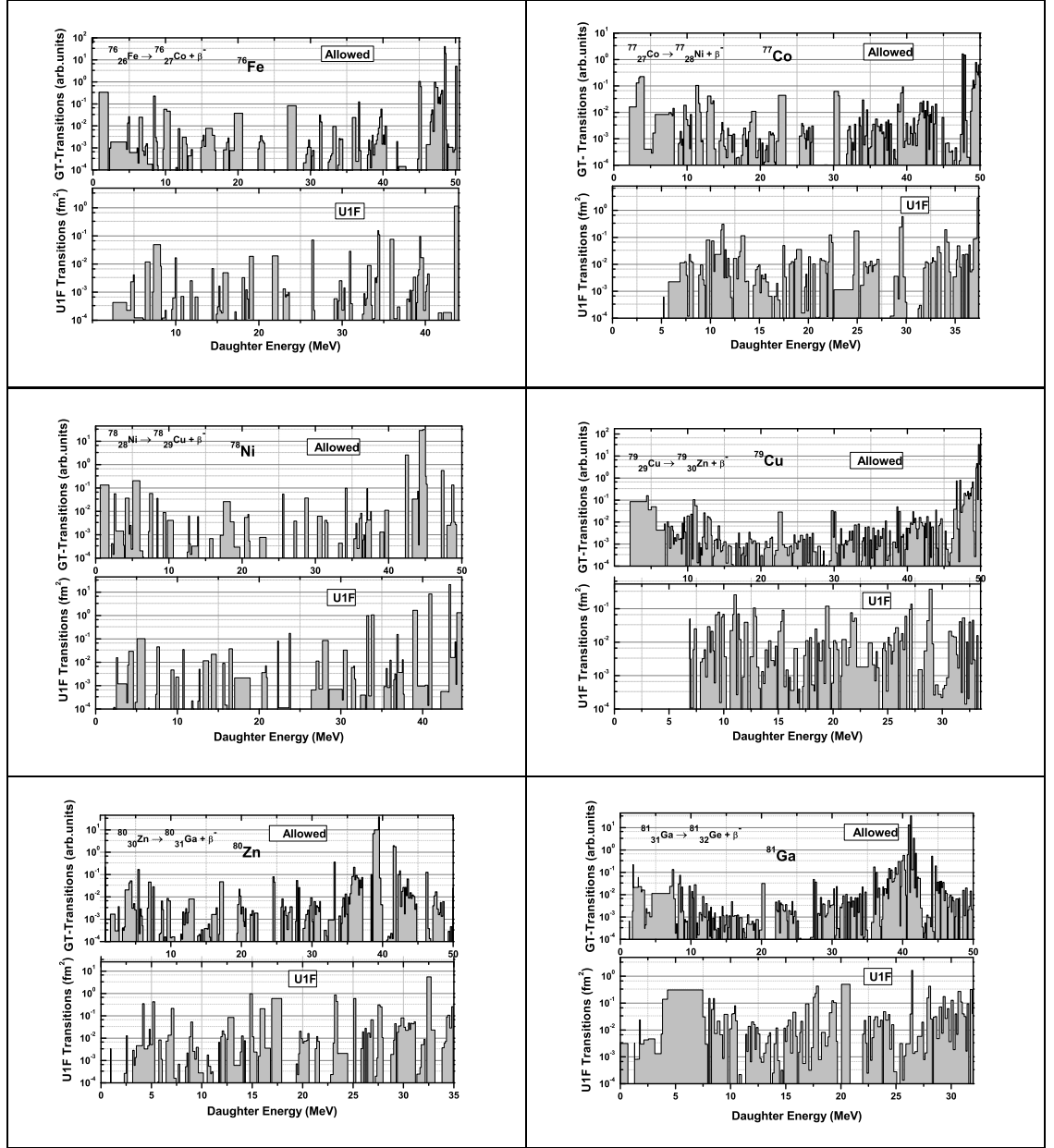


Figure 13: Allowed and unique-first forbidden (U1F) β -decay transitions for ^{76}Fe , ^{77}Co , ^{78}Ni , ^{79}Cu , ^{80}Zn and ^{81}Ga as a function of daughter excitation energy calculated using the pn-QRPA model.

to the total weak rates for $N = 82$ waiting point nuclei.

The skyscrapers for the calculated charge-changing strength distribution along β -decay direction for the ten waiting point nuclei are shown in Fig. 13

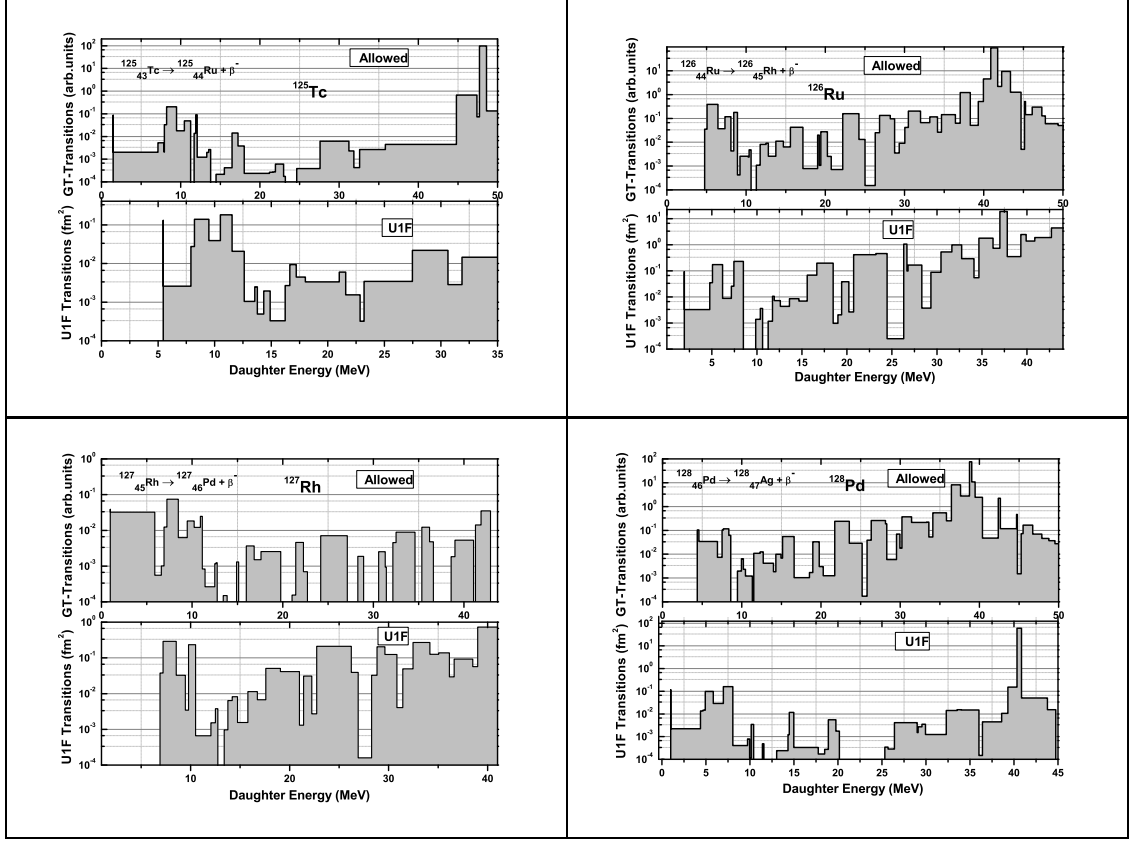


Figure 14: Same as Fig. 13 but for ^{125}Tc , ^{126}Ru , ^{127}Rh and ^{128}Pd .

and Fig. 14. For each nucleus, the bottom panel shows the U1F transitions and the upper panel the allowed GT transitions, respectively. We again mention that all our calculated strength were quenched by a factor of $f_q^2 = (0.55)^2$ [36]. It may be noted that the pn-QRPA model calculates high lying allowed GT transitions for all nuclei. This is also verified by the large values calculated values of centroid shown in Table 4. The U1F transitions were calculated to relatively lower excitation energies in daughter. This trend was also noted in the calculation of [20]. It is noted in Fig. 13 that U1F transitions are comparable in magnitude with the allowed GT transitions for ^{78}Ni and ^{80}Zn . This is the reason that the terrestrial half-life is reduced by $\sim 50\%$ when U1F transitions were incorporated in pn-QRPA calculation (see Table 1). We note significant contribution from U1F transitions for the $N = 82$ cases (Fig. 14). For the even-even cases, ^{126}Ru and ^{128}Pd , this substantial U1F contribution resulted in more than 95% reduction in calculated terrestrial half-lives (see Table 1). For the case of ^{127}Rh , once again the U1F contribution is very significant but from Table 1 the half-

life is reduced only by 32%. The reason for this is traced back to phase space calculation where it is seen from Fig. 12 that at $T_9 = 0.01$ (at this low temperature, stellar phase space would very much mimic the terrestrial phase space) the U1F phase space is roughly an order of magnitude smaller than the allowed phase space.

4 Summary and Conclusions

For the first time we present the allowed GT and U1F weak rates of $N = 50$ and $N = 82$ waiting point nuclei in stellar environment using the deformed pn-QRPA model. We quenched our calculated charge-changing transition by a quenching factor of $f_q^2 = (0.55)^2$. The calculated charge-changing strength distributions, phase space and weak rate calculations, separately for allowed and U1F transitions, were presented for a total of ten r -process waiting point nuclei. High lying centroids were computed for the calculated allowed GT strength distributions. Our calculation fulfilled the model-independent Ikeda sum rule, except for a couple of odd-A cases. The pn-QRPA calculated half-lives, after incorporation of U1F transitions, were in decent agreement with the measured half-lives and at the same time were also suggestive of incorporation of non-unique forbidden contributions which we plan to take as a future assignment. It is hoped that the present study would prove useful for a better and reliable simulation of nucleosynthesis calculation.

We found substantial U1F contribution to the β -decay half-lives for the $N = 82$ waiting points. Except for ^{127}Rh , the calculated U1F stellar rates were orders of magnitude bigger than allowed GT rates at high stellar temperatures approaching $T_9 = 30$.

The neutrino-driven wind streaming out of the neutron star forming at the center of a type II supernova has been shown to be one of possible candidates for the site of r -process. If r -process happened in a neutron-rich environment, then the electron neutrino capture could compete with the β -decay rates and is capable of modifying the r -abundance distribution by subsequent ν -induced neutron spallation. We plan to calculate the charged-current electron neutrino capture as a future assignment.

The weak rates for all ten waiting point nuclei, as a function of stellar temperature and density, are available as ASCII files and may be requested from the corresponding author.

Acknowledgment: J.-U. Nabi would like to acknowledge the support of the Higher Education Commission Pakistan through the HEC Project No. 20-3099.

References

- [1] E.M. Burbidge, G.R. Burbidge, W.A. Fowler and F. Hoyle, *Synthesis of the elements in stars*, *Rev. Mod. Phys.* **29** (1957) 547.
- [2] R.H. Cyburt, B.D. Fields, K.A. Olive and T.H. Yeh, *Big bang nucleosynthesis: Present status*, *Rev. Mod. Phys.* **88** (2016) 015004.
- [3] K. Nomoto, C. Kobayashi and N. Tominaga, *Nucleosynthesis in stars and the chemical enrichment of galaxies*, *Ann. Rev. Astron. Astro.* **51** (2013) 457.
- [4] J.J. Cowan, F.-K. Thielemann and J.W. Truran, *The r-process and nucleochronology*, *Phys. Rep.* **208** (1991) 267.
- [5] M. Arnould and K. Takahashi, *Nuclear astrophysics*, *Rep. Prog. Phys.* **62** (1999) 395.
- [6] K.-L. Kratz, J.P. Bitouzet, F.-K. Thielemann, P. Möller and B. Pfeiffer, *Isotopic r-process abundances and nuclear structure far from stability-Implications for the r-process mechanism*, *Astrophys. J.* **403** (1993) 216.
- [7] S.E. Woosley, G.J. Mathews, J.R. Wilson, R.D. Hoffman and B.S. Meyer, *The r-process and neutrino-heated supernova ejecta*, *Astrophys. J.* **433** (1994) 229.
- [8] K.-L. Kratz, F.-K. Thielemann, W. Hillebrandt, P. Möller, V. Härms, A. Wöhr and J.W. Truran, *Constraints on r-process conditions from beta-decay properties far off stability and r-abundances*, *J. Phys. G* **24** (1988) S331.
- [9] P.T. Hosmer *et al.*, *Half-life of the doubly magic r-process nucleus ^{78}Ni* , *Phys. Rev. Lett.* **94** (2005) 112501.
- [10] K.-L. Kratz *et al.*, in *Proceedings of the International Conference on Fission and Properties of Neutron-Rich Nuclei*, Sanibel Island, 1997, edited by J.H. Hamilton *World Scientific Press, Singapore*, (1998).
- [11] K.-L. Kratz, H. Gabelmann, W. Hillebrandt, B. Pfeiffer, K. Schlösser and F.-K. Thielemann, *The Beta-decay half-life of $^{130}_{48}\text{Cd}_{82}$ and its importance for astrophysical r-process scenarios*, *Zeitschrift für Physik A Atomic Nuclei* **A 325** (1986) 489.
- [12] B. Pfeiffer, K.-L. Kratz, F.-K. Thielemann and W.B. Walters, *Nuclear structure studies for the astrophysical r-process*, *Nucl. Phys.* **A 693** (2001) 282.

- [13] S. Nishimura *et al.*, β -Decay half-lives of very neutron-rich Kr to Tc isotopes on the boundary of the r -process path: An indication of fast r -matter flow, *Phys. Rev. Lett.* **106** (2011) 052502.
- [14] T. Kurtukian-Nieto *et al.*, Recent progress in measuring β half-lives of nuclei approaching the r -process waiting point $A=195$, *Nucl. Phys. A* **827** (2009) 587C.
- [15] H.V. Klapdor-Kleingrothaus, J. Metzinger and T. Oda, Beta-decay half-lives of neutron-rich nuclei, *ADNDT* **31** (1984) 81.
- [16] A. Staudt, E. Bender, K. Muto and H.V. Klapdor-Kleingrothaus, Microscopic calculations of beta decay far from stability, *Zeitschrift für Physik A Atomic Nuclei* **334** (1989) 47.
- [17] A. Staudt, E. Bender, K. Muto and H.V. Klapdor-Kleingrothaus, Second-generation microscopic predictions of beta-decay half-lives of neutron-rich nuclei, *ADNDT* **44** (1990) 79.
- [18] M. Hirsch, A. Staudt, K. Muto and H.V. Klapdor-Kleingrothaus, Microscopic predictions of β^+ /EC-decay half-lives, *ADNDT* **53** (1993) 165.
- [19] H. Homma, E. Bender, M. Hirsch, K. Muto, H.V. Klapdor-Kleingrothaus and T. Oda, Systematic study of nuclear β -decay, *Phys. Rev. C* **54** (1996) 2972.
- [20] P. Möller, B. Pfeiffer and K.-L. Kratz, New calculations of gross β -decay properties for astrophysical applications: Speeding-up the classical r process, *Phys. Rev. C* **67** (2003) 055802.
- [21] I.N. Borzov, β -delayed neutron emission in the ^{78}Ni region, *Phys. Rev. C* **71** (2005) 065801.
- [22] Q. Zhi, E. Caurier, J.J. Cuenca-García, K. Langanke, G. Martínez-Pinedo and K. Sieja, Shell-model half-lives including first-forbidden contributions for r -process waiting-point nuclei, *Phys. Rev. C* **87** (2013) 025803.
- [23] J.-U. Nabi and H.V. Klapdor-Kleingrothaus, Microscopic calculations of weak interaction rates of nuclei in stellar environment for $A=18$ to 100 , *Eur. Phys. J. A* **5** (1999) 337.
- [24] J.-U. Nabi and H.V. Klapdor-Kleingrothaus, Weak interaction rates of sd -shell nuclei in stellar environments calculated in the proton-neutron quasiparticle random-phase approximation, *ADNDT* **71** (1999) 149.
- [25] J.-U. Nabi and H.V. Klapdor-Kleingrothaus, Microscopic calculations of stellar weak interaction rates and energy losses for fp - and fpg -shell nuclei, *ADNDT* **88** (2004) 237.

- [26] N.B. Gove and M.J. Martin, *Log-f tables for beta decay*, *ADNDT* **10** (1971) 205.
- [27] J.-U. Nabi, N. Çakmak, Z. Iftikhar, *First-forbidden β -decay rates, energy rates of β -delayed neutrons and probability of β -delayed neutron emissions for neutron-rich nickel isotopes*, *Eur. Phys. J. A* **52** (2016) 1.
- [28] M. Wang, G. Audi, A.H. Wapstra, F.G. Kondev, M. MacCormick, X. Xu and B. Pfeiffer, *The Ame2012 atomic mass evaluation*, *Chin. Phys. C* **36** (2012) 1603.
- [29] P. Möller, J.R. Nix, W.D. Myers and W.J. Swiatecki *Nuclear ground-state masses and deformations*, *ADNDT* **59** (1995) 185.
- [30] B. Pfeiffer, K.-L. Kratz and P. Möller, *Status of delayed-neutron precursor data: half-lives and neutron emission probabilities*, *Prog. Nucl. Energy* **41** (2002) 39.
- [31] P. Möller, J.R. Nix and K.-L. Kratz, *Nuclear properties for astrophysical and radioactive-ion-beam applications*, *ADNDT* **66** (1997) 131.
- [32] S. Cakmak, J.-U. Nabi, T. Babacan and I. Maras, *Spin-isospin transitions in chromium isotopes within the quasiparticle random phase approximation*, *Adv. Space Research*, **55** (2015) 440.
- [33] K. Langanke and G. Martínez-Pinedo, *Nuclear weak-interaction processes in stars*, *Rev. Mod. Phys.* **75** (2003) 818.
- [34] J.J. Cuenca-García, G. Martínez-Pinedo, K. Langanke, F. Nowacki and I. Borzov, *Shell model half-lives for r -process $N = 82$ nuclei*, *Eur. Phys J. A* **34** (2007) 99.
- [35] G. Audi, M. Wang, A.H. Wapstra, F.G. Kondev, M. MacCormick, X. Xu and B. Pfeiffer, *The Ame2012 atomic mass evaluation*, *Chin. Phys. C* **36** (2012) 1287.
- [36] J.-U. Nabi and M.-U. Rahman, *Gamow-Teller transitions from ^{24}Mg and their impact on the electron capture rates in the $O+Ne+Mg$ cores of stars*, *Phys. Rev. C* **75** (2007) 035803.

